

# We are IntechOpen, the world's leading publisher of Open Access books Built by scientists, for scientists

6,900

Open access books available

185,000

International authors and editors

200M

Downloads

Our authors are among the

154

Countries delivered to

TOP 1%

most cited scientists

12.2%

Contributors from top 500 universities



WEB OF SCIENCE™

Selection of our books indexed in the Book Citation Index  
in Web of Science™ Core Collection (BKCI)

Interested in publishing with us?  
Contact [book.department@intechopen.com](mailto:book.department@intechopen.com)

Numbers displayed above are based on latest data collected.  
For more information visit [www.intechopen.com](http://www.intechopen.com)



# Versatile and Scalable Approaches to Tune Carbon Black Characteristics for Boosting Adsorption and VOC Sensing Applications

*Michela Alfè and Valentina Gargiulo*

## Abstract

This chapter explores the potential use of carbon black (CB) as point of departure to design a highly varied array of materials with practical applications in energetics, remediation, and sensoristics. Thanks to its graphenic moieties embedded in a nanostructured backbone, CB is prone to be structurally and chemically modified exploiting quite mild chemical conditions. The proposed approaches, implying an easy tuning of the chemo-physical properties to the specific needs, are thought up to meet urgent sustainability needs: low costs, scalability, and flexibility. In this chapter, we will describe the modification of CB at the surface (i.e., introduction of oxygen functional group, functionalization, coating with active phases) and a highly CB deconstruction to produce graphene-related materials (GRMs) suitable for film production and for the designing of new hybrid materials. CB is converted into highly homogenous CB-modified nanoparticles (around 160 nm) with adjustable surface properties (hydrophilicity, type and surface charge density, pore size distribution) and in highly versatile GRMs for the production of structured electrical conductive ultrathin films for trace alcohol sensing and a wide array of hybrid materials, including photocatalysts (carbon-iron oxide, silica-carbon, carbon-titanium oxide hybrids) for adsorption applications (CO<sub>2</sub> capture, heavy metal capture).

**Keywords:** carbon black, advanced materials, graphene-related materials, ultrathin films, hybrid materials, sensing layers

## 1. Introduction

Carbons blacks (CB) are carbonaceous materials [1] broadly classified as industrial aciniform aggregates (IAA) in which the smallest dispersible unit consists of grapelike aggregates. They are mostly produced from controlled thermal processes mainly starting from crude oils or natural gas. The different manufacture processes designate the different kinds of CB, each of them characterized by specific morphologies and chemo-physical properties [1]. The most widely used production processes, providing CB with a highly controlled morphology, are oil furnace (also known as furnace black process) and thermal black processes in which heavy aromatic oils and

natural gas (methane is the mostly used feedstock) or higher-grade hydrocarbon oils are pyrolyzed (furnace CB) and thermally decomposed (thermal CB), respectively. CB are also produced by channel black process (providing crude oil-generated CB pigments with very fine particles characterized by a high content of oxygen-containing surface groups), lamp black process (the oldest way to produce CB, not suitable for mass production, providing CB with specific color from oil lamp or pinewood heating), and acetylene black process (providing a high-purity, high-crystalline, and electric conductive CB by thermally decomposing acetylene gas) [2, 3].

CB are composed almost exclusively by elemental carbon (>97 wt.%) with a minor and variable amount of hydrogen, oxygen, and sulfur (less than 1% each); usually the hydrogen to carbon atomic ratio (H/C) is less than 0.05 [2, 4]. Trace amounts of adsorbed organic compounds (polycyclic aromatic hydrocarbons and aliphatic/aromatic hydrocarbons) and inorganic impurities (salts of alkali and alkaline earth metals) as manufacturing residuals can also be found [4].

At the nanoscale level, CB is composed almost exclusively of stacked sheets of condensed aromatic ring systems (i.e., graphene layers), concentrically arranged and oriented around a central core to form almost spherical primary particles (from 10 to 300 nm, in dependence of the manufacturing). Primary particles are fused into grapelike-shaped aggregates (aciniform aggregates, usually less than 500 nm) representing the discrete, dispersible CB smallest unit. Aggregates clustered in the so-called agglomerates.

CB are usually highly agglomerated, with 10–1000 aggregates per agglomerate. The three-dimensional configuration of the CB aggregates results in varied but usually large surface areas (SA) (5–200 m<sup>2</sup>/g).

The size of the primary particle and the degree of aggregation differentiate the grades of carbon black [2]. The CB microstructure (microtexture, particle size, and the morphology of aggregates) is regarded as the key property to allocate the proper commercial use of a specific carbon black [2].

The edge of CB graphenic layers is chemically reactive and can be decorated with specific functional groups, while the basal planes are quite less reactive. Several evidences have confirmed the presence of H atoms as well as four types of oxygen-containing functional groups on the as-produced CB surface: lactones, phenolic, carboxylic, and carbonylic groups [5, 6]. Such chemical groups are considered to be essential for the chemical manipulation of CB powder in mild conditions since they modulate CB solvent suspendibility.

Furnace black is the most commonly used CB (almost 95% of the total market) as it is widely applied in tire and other related automotive manufacture, while only some specific typologies of thermal black find application in rubber production. Although CB are massively used in ink and rubber industry, noteworthy emerging CB applications are the production of sensitive components in electrochemical sensors [7], the production of counter electrodes for dye-sensitized solar cells [8], the production of hybrid photocatalysts [9] and composites with heat insulating properties [10], the development of electrically conductive fabrics for wearable heating applications [11], and the development of construction materials with improved physical properties (i.e., electrical conductivity) [12, 13].

In our approach, we explored the production of a highly varied array of advanced materials starting from a furnace CB and using feasible approaches designed to meet the continuous need of low-cost and scalable protocols for tuning easily the relevant chemo-physical properties of the desired carbon-based materials.

An extensive experimental campaign has been conducted since many years in our group on a CB N110 type (furnace black, **Figure 1**).

This CB is characterized by a H/C atomic ratio of 0.058, a density of 1.8 g/mL at 25°C, and an inorganic content less than 0.1 wt.%. It is a meso-porous material

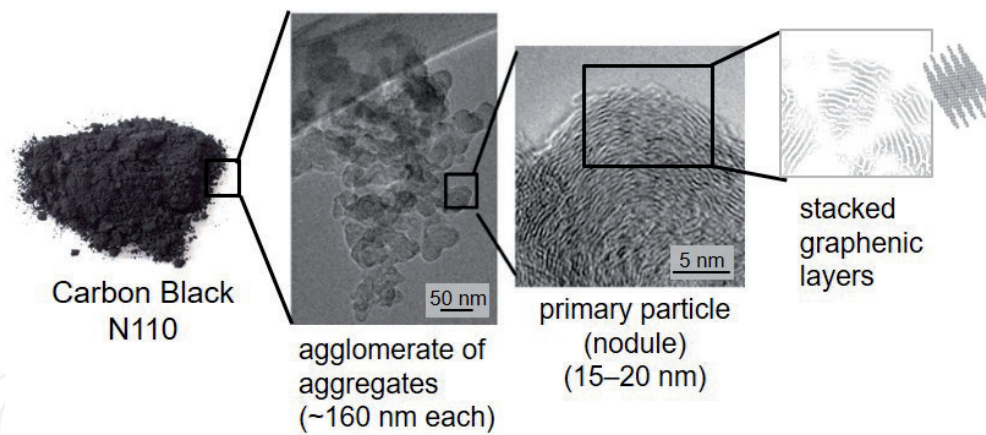


**Figure 1.**  
Structure of a CB N110 (furnace black) from macro- to nanoscale.

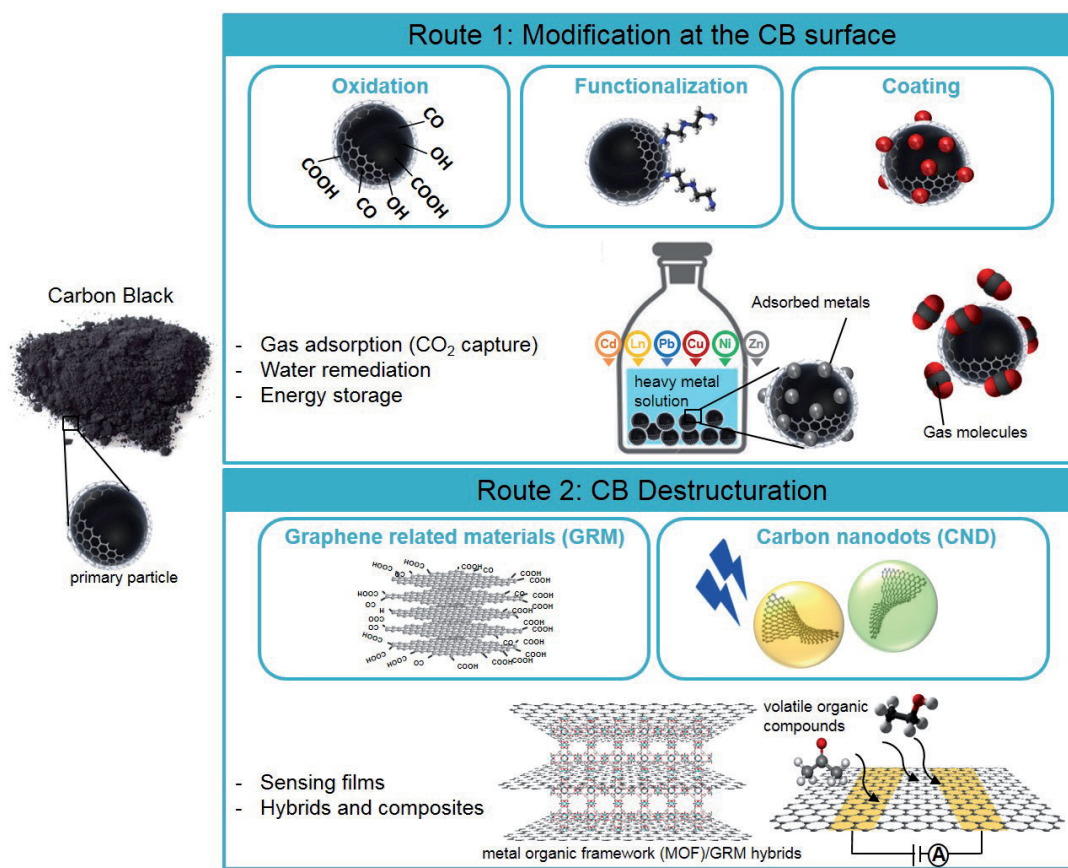


**Figure 2.**  
Advanced materials produced from CB N110 and their applications in sensing and remediation fields.

with a SA of 139 m<sup>2</sup>/g. Its microstructure is organized in chain-like aggregates with a hydrodynamic diameter, measured by dynamic light scattering (DLS), of 160 ± 20 nm. The diameter of the aggregate building blocks (primary particles or nodules) is 15–20 nm [14, 15].

Two main routes have been exploited starting from the as-produced CB N110 (hereinafter CB) (**Figure 2**) [16]:

- i. Modification and introduction of specific chemical functional groups at the CB surface (modification at the CB surface).
- ii. Extraction of graphenic nanoplatelets from CB backbone (CB destructuration).



The first route allows to produce CB-modified nanoparticles having narrow hydrodynamic diameter ( $160 \pm 10$  nm) and customized surface properties (hydrophilicity, type and surface charge density, SA, and pore size distribution). These CB-derived materials have been mainly designed as adsorbents for heavy metal removal (thanks to the presence of oxygen functional groups) and as supports for ionic liquid (SILP) and for magnetic iron oxide particles (thanks to their meso-porosity).

The second route is framed as a top-down approach and leads to the demolition of CB backbone to obtain water-stable graphene-related materials (GRM) as (i) stacked graphene-like layers (GL), highly functionalized to serve as building blocks for producing a wide array of advanced hybrid materials and ultrathin self-assembling carbon-based films, and (ii) yellow and green fluorescent carbon nanodots (the latter at the early stage of the experimentation).

In the following, details on the synthetic approaches, the structural characteristics, and potential applications of the developed materials in environmental fields (sensing and remediation) are reported.

## **2. Modification of CB at the surface**

### **2.1 Colloidal hydrophilic nanoparticles (carboxyl enriched)**

The oxidative treatment of CB with hot nitric acid allows to produce colloidal hydrophilic nanoparticles (HNPs) with uniform size bearing on the surface oxygen-containing acidic sites (mainly carboxylic groups but also lactone, lactol, and phenol groups) [6, 15, 17] whose amount depends on the oxidative treatment time (the total number of oxygen-containing functional groups varies from  $1.56 \pm 0.10$  mmol/g to  $2.25 \pm 0.08$  mmol/g upon 4 and 24 h of treatment, respectively). The wet chemistry treatment, performed up to 24 h of reaction time, generates nanoparticles with an increasing oxygen content: from 0.59 wt.% in as-produced CB up to 31.8 wt.% after 24 h of reaction time [15]. A higher reaction time does not lead to a significant gain in oxygenation degree (further discussed in detail later on) as testified by the product obtained after 90 h of treatment characterized by an oxygen content of 44.1 wt.% [17].

Interestingly, the acid treatment up to 24 h does not alter the hydrodynamic diameter of the aggregate (around  $165 \pm 10$  nm in all the explored cases) and significantly improves the volumes of both micro- and meso-pores [15] thus enhancing the surface area from  $139 \text{ m}^2/\text{g}$  (raw CB) up to  $323 \text{ m}^2/\text{g}$  (after 24 h of treatment).

The HNPs obtained after treatments lasting between 4 and 24 h exhibited a good colloidal stability in water and in a wide pH range (from 4 to 12) [6, 15] and were found highly exploitable for heavy metal removal including rare-earth elements (Ln(III) ions) [6, 15].

Their capacity to reversibly adsorb heavy metals was verified through batch experiments by using cadmium, nickel, lead, and zinc as target metals [6, 15, 17]. In the case of cadmium, an appreciable adsorption capacity at different temperatures ( $10$ – $60^\circ\text{C}$ ) and in a wide range of pH ( $2$ – $6$ ) has been verified [15]. A good correlation between the concentration of active sites (specifically carboxylic functional groups) on the HNP surface and the cadmium adsorption capacity was also highlighted [15]. Interestingly enough, the HNPs exhibited good cadmium capture also at low concentration: this circumstance is noticeable since in water depuration the actual adsorption capacity close to the allowed discharge limit is a

very important parameter. In particular, accordingly with the Italy's current regulations that fix the limit for sewage discharge at 0.2 mg/L [18], it was established that the cadmium adsorption capacity at 20°C and pH 3.5 (selected by taking into account that most of the cadmium wastewaters are acidic) was 3.84 mg/g for HNP at the higher oxygenation degree (24 h of hot acidic treatment) [15]. These values resulted comparable or superior with respect to commercial activated carbons (even those oxidized), ashes, and residual solids but similar or far lower than specific sorbents from biosources (activated char) or polyacrylonitrile (PAN) fibers [15].

The heavy metal sorption mechanism on HNPs has been also investigated by combining X-ray fluorescence, infrared spectroscopy, and differential pulse voltammetry at  $\text{pH} \leq 6$  [6]. The experiments suggested that the adsorption of metal ions on HNPs is controlled by chemical adsorption involving a strong complexation of metal ions with the carboxylic groups on the surface of HNPs.

Moreover, the good surface complexation of lanthanum ions on HNP surface highlighted by this study opens the possibility to feasibly exploit HNPs in solid-phase extraction for the pre-concentration, separation, and quantification of rare-earth elements, also including actinides [6].

As mentioned before, the HNPs are highly stable in water over a wide pH range given the establishment of colloidal stable suspensions, causing difficulties in the separation of HNPs from water. To overcome this limitation, micrometric-sized carbon-silica hybrids (SHNPs) have been designed, developed, and tested for heavy metal adsorption [15, 17]. The HNPs were firmly supported over silica thanks to the tight interactions between the oxygen functional groups borne by the HNP and the hydrophilic silica surface. The carbon-silica hybrids can be easily filtered from wastewater with conventional filter units, and, moreover, they can be used also in applications at pH values higher than those explored with bare HNPs [15], thus paving the way to a feasible use of these sorbents for heavy metal adsorption in commercial units [15, 17].

HNPs obtained after different times of oxidation (from 0.5 up to 90 h) have been used for the preparation of different SHNPs. The adsorption capacity of HNPs supported over silica toward Cd(II) (representative of a soft acid) and Ni(II) ions (representative of an intermediate acid) [19] has been determined through batch experiments exploring the effects of the most relevant process parameters (solution temperature, pH, and initial concentration of the target metal) [17]. The effect of different sorbent preparations (HNP oxidation time and loading of active phase over the silica support) was also thoroughly investigated [17]. The SHNPs exhibited high removal efficiencies for the three metals at neutral pH and low temperature (10°C), conditions typically adopted for natural water and for some industrial wastewater remediation (**Figure 3**).

As a consequence of the presence of the carboxylic functional groups on the HNP surface, the SHNPs resulted more selective toward Ni(II) ions, which behave as an intermediate acid, than toward Cd(II) ions, which behave as a soft acid. Among Cd(II) and Pb(II) ions, the latter exhibited the lowest adsorption efficiency [17].

The sorbents exhibited high adsorption capacities per gram of active phase: considering the silica-based material obtained with the HNPs produced after 24 h of oxidation, the following adsorption capacities have been measured: 13.48 mg/g for Ni(II) ions, which is far higher than those of other sorbents available in the literature, 0.54 mg/g for Cd(II) ions, and 8.87 mg/g for Pb(II) ions [17].

Modeling analysis on the adsorption isotherms revealed that the Gibbs free energy of interactions between the sorbent and Ni(II) and Pb(II) ions is higher

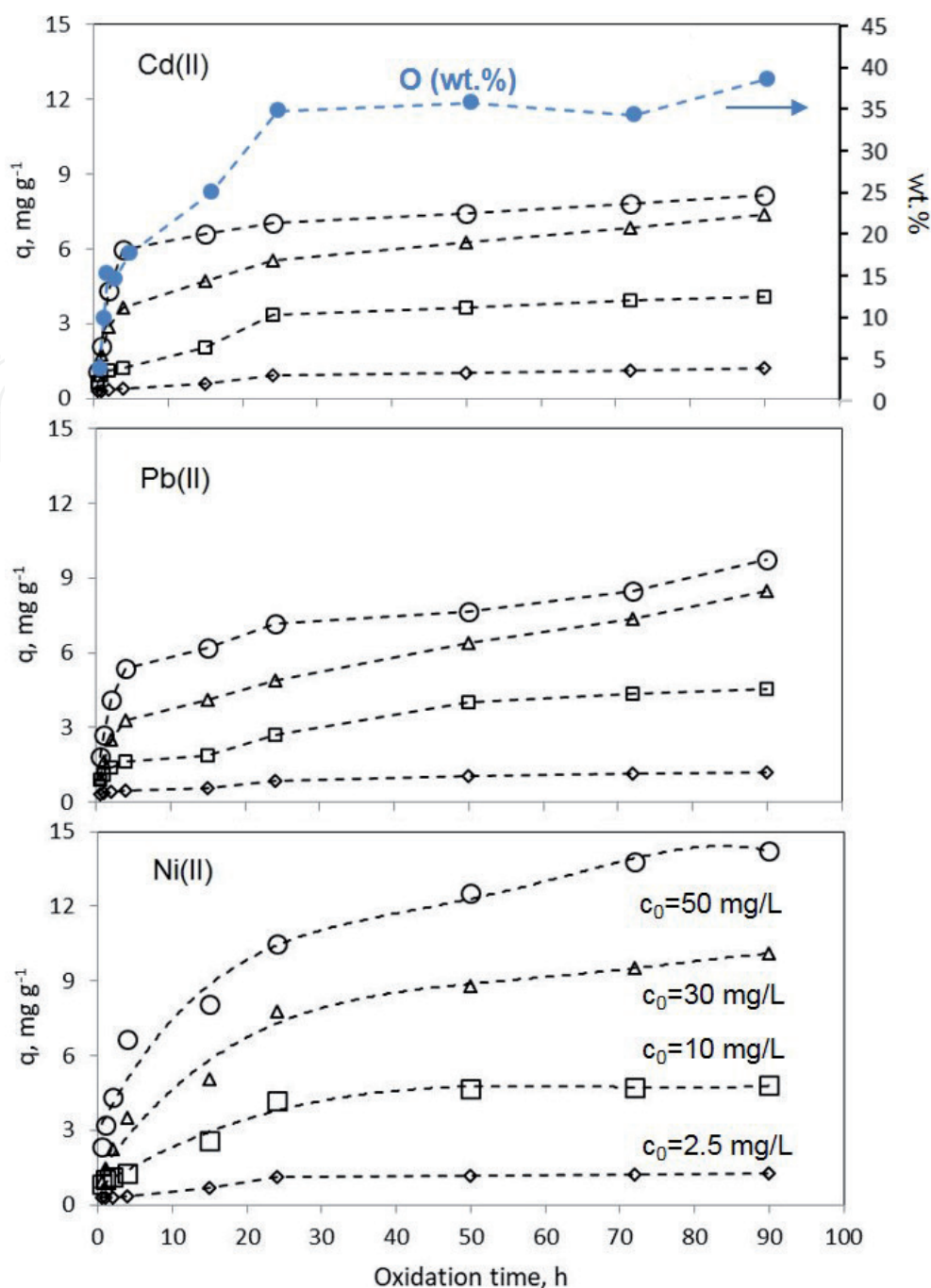


**Figure 3.** Adsorption capacities of SHNPs toward  $\text{Cd(II)}$ ,  $\text{Pb(II)}$ , and  $\text{Ni(II)}$  ions as a function of CB oxidation time. Experimental conditions: 5 wt.% HNP loading,  $T = 25^\circ\text{C}$ ,  $m/V = 40 \text{ g/L}$ ;  $\diamond C_0 = 2.5 \text{ mg/L}$ ;  $\square C_0 = 10 \text{ mg/L}$ ;  $\Delta C_0 = 30 \text{ mg/L}$ ;  $\circ C_0 = 50 \text{ mg/L}$ . The oxygen content (wt.%) of the corresponding HNPs is also reported (blue dots) (adapted from [17]).

than that of  $\text{Cd(II)}$  ions indicating that the sorbents are more affine to intermediate acids, as  $\text{Ni(II)}$  and  $\text{Pb(II)}$  ions, than to soft acids, as  $\text{Cd(II)}$  ions [17].

As concerns the effect of sorbent preparation parameters, it is worth of note that an active phase obtained after 90 h of oxidation with respect to a phase obtained after 24 h may provide an increase in the adsorption capacity of  $\text{Ni(II)}$  and  $\text{Pb(II)}$  ions by an additional 30%, while no other benefits have been sought for  $\text{Cd(II)}$  ions.

## 2.2 Surface-modified CB (carboxyl and amino-derivatives, $\text{CB/Fe}_3\text{O}_4$ , supported ionic liquids)

Since 2005 the widespread carbon capture and storage (CCS) program aims to prevent the effects of carbon dioxide emissions. The CCS concept is a multistep and



multidisciplinary process based on (i) catching CO<sub>2</sub> from massive sources, such as fossil fuel-based power plants; (ii) transportation to the designed place of storage; and (iii) stable storage where it will not get to the atmosphere, usually underground geological formations [20].

As concerns the first step, to date three methods of capturing CO<sub>2</sub> directly from industrial sources are known post-combustion capture, precombustion capture, and combustion of fossil fuels in a pure oxygen environment [20]. Samanta et al. indicate that post-combustion capture of CO<sub>2</sub> from flue gas is one of the key technological options to meet the need of reducing greenhouse gases in the short-term period, because the capture units can be potentially added without substantially modifying at all the existing fleet of coal-fired power plants [21]. The most performing post-combustion carbon capture processes include amine-based absorption, ammonia-based absorption, solid sorbent adsorption, and membrane filtration [20].

Adsorption processes using solid sorbents capable of capturing CO<sub>2</sub> from flue gas streams have shown many potential advantages, compared to other conventional CO<sub>2</sub> capture approaches as aqueous amine solvents.

The use of solid sorbents is one of the most promising options for post-combustion CO<sub>2</sub> capture strategies [21] since it assures (i) reduced energy consumption for regeneration, (ii) great capacity, (iii) selectivity, and (iv) ease of handling. In this framework, the specific characteristics required by a good CO<sub>2</sub> adsorbent are (i) production and regeneration at reduced (or, at least, economically convenient) costs; (ii) selectivity toward CO<sub>2</sub> over the typical flue gas components; and (iii) chemical and mechanical stability to undergo repeated CO<sub>2</sub> sorption/desorption cycles over a wide range of temperatures and pressures [22].

Overall, materials with a distinctive surface chemistry and defined porosity (pore diameter below 1 nm) find large applications in CCS technologies [21–24]. In the manifold of inorganic materials suitable for CO<sub>2</sub> capture applications, ferric oxide nanoparticles represent a cost-effective CO<sub>2</sub> sorbent, thanks to the presence of surface coordinatively unsaturated metal and O sites favoring the instauration of acid–base interactions (Lewis type) with the acidic CO<sub>2</sub> molecule. The interaction between the active sites on iron oxide surface and CO<sub>2</sub> leads to the formation of adsorbed carbonates, bicarbonates and carboxylates, as well as bent CO<sub>2</sub> species [25–27]. The efficient use of ferric oxide as CO<sub>2</sub> adsorbent under post-combustion CO<sub>2</sub> capture conditions is hampered by the tendency to form agglomerates with lower surface area and lower gas capture efficiency. To limit this issue, the dispersion of ferric oxide nanoparticles over a carbonaceous matrix (activated carbons, carbon nanotubes, graphite oxide) is successfully adopted [26, 27]. CB has been proposed as carbonaceous support for iron oxide (specifically magnetite, Fe<sub>3</sub>O<sub>4</sub>, FM) to produce hybrid sorbents for CO<sub>2</sub> capture applications [28–30]. In this framework hybrid materials were synthesized applying a one-pot synthetic approach based on a coprecipitation strategy allowing the iron oxide particles to form in presence of CB [28, 29]. In this way a homogeneous incorporation of both the carbonaceous material and the iron oxide particles into the hybrid materials was obtained. A series of CB/FM hybrids was produced by varying the CB to FM ratio. The obtained materials exhibited a comparable SA (around 150 m<sup>2</sup>/g) and tunable pore size distributions [28]. More specifically, the pore size distribution ranges from the porosity typical of FM (20–50 Å) for low-CB-containing hybrids (up to 14 wt.% of CB load) to the CB pore size distribution typically broadly centered around 200 Angstroms (for hybrid containing CB more than 60 wt.% of CB) [28]. The CO<sub>2</sub> uptakes of the different hybrids were evaluated in a lab-scale fixed bed reactor under dynamic conditions using typical post-combustion conditions (CO<sub>2</sub> 3–10% vol. and atmospheric pressure). It was established that the CO<sub>2</sub> uptake



reached the highest values when the amount of CB in the hybrid ranged between 14.3 and 60 wt.%. This finding indicated that a synergistic effect between the two components (CB and FM) has been reached. It was also demonstrated that both the material surface area (accounting for physisorption phenomena) and surface chemical features of iron oxide particles (accounting for chemisorption phenomena) have relevance [28, 30].

In order to have a clear idea of the potential of the CB/FM hybrids, the sorbent exhibiting the highest adsorption capacity (50 wt.% of CB load, 16.5 mg<sub>CO<sub>2</sub></sub>/g at  $C_0(\text{CO}_2) = 3\%$  vol., and inlet flow rate = 15 NL/h) was tested in a prototypal sound-assisted fluidized bed [28]. The fluidization technology was adopted for this testing since it is generally considered to be one of the best available techniques to handle and process large quantities of powders. Since the fluidization of fine powders (as CB/FM hybrids, since the particle size distribution is lower than 40  $\mu\text{m}$  with a Sauter diameter of about 350 nm) is expected to be particularly difficult, sound-assisted fluidization was used to achieve a smooth fluidization regime by overcoming the interparticle forces.

The testing of the selected sorbent was carried out operating the sound-assisted fluidized bed apparatus under post-combustion conditions ( $C_0(\text{CO}_2) = 10\%$  vol.; inlet flow rate = 67.8 NL/h; sound intensity = 140 dB; sound frequency = 80 Hz) also exploring in situ regeneration and cyclability (desorption temperature = 250°C). In such conditions the CO<sub>2</sub> uptake was considerably enhanced up to about 20 mg<sub>CO<sub>2</sub></sub>/g. The experimental campaign demonstrated also that the material underwent several CO<sub>2</sub> adsorption and desorption cycles without losing in performances. It is noteworthy that the time needed to adsorb 95% of the total CO<sub>2</sub> uptake (about 11 min) is comparable to the required to completely regenerate the sorbent, opening the possibility to operate cyclically in two interconnected fluidized beds [28].

The best performing hybrid (50 wt.% of CB load) was fully characterized from both thermodynamic and kinetic points of view under dynamic conditions [31, 32]. More in detail, the CO<sub>2</sub> adsorption data collected under isothermal conditions (18–150°C) and with CO<sub>2</sub> partial pressure ranging between 0.5 and 20 vol.% [31] showed that adsorption temperature and pressure have opposite effects on the thermodynamics of the process: the CO<sub>2</sub> adsorption capacity increases with increasing pressure, and it decreases with increasing temperature. The Freundlich and Toth models allowed the best fits of the CO<sub>2</sub> adsorption data suggesting that a multilayer process characterized by a heterogeneous surface binding takes place. Finally, the CO<sub>2</sub> adsorption on the selected CB/FM hybrid was found to be a spontaneous and exothermic process based neither on purely physisorption nor on purely chemisorption [31]. From the kinetic point of view, the mechanism of CO<sub>2</sub> adsorption on the selected CB/FM hybrid has been investigated in terms of controlling mass transfer resistances, interparticle diffusion, intraparticle diffusion, and Boyd's film-diffusion models [32]. The results showed that mass transfer during CO<sub>2</sub> adsorption on CB/FM proceeds through a diffusion-based process involving three different successive steps: film diffusion, intraparticle diffusion, and surface reaction once equilibrium is approaching. The adsorption and desorption data have been also fitted with different models, and the best fit has been obtained using Avrami's model, as it is capable of accounting for a hybrid CO<sub>2</sub> adsorption mechanism stemming from two different pathways, i.e., physisorption and chemisorption [32].

The experimental campaigns conducted on CB/FM hybrids [28] highlighted that also in CO<sub>2</sub> adsorption under dynamic conditions, the surface area of the carbonaceous support and, more specifically, the distribution of micro- and meso-pores play a relevant role. To go deep into this issue, raw CB has been worked out to expose a different porosity (and surface chemistry features) and explored as a solid support for different typologies of CO<sub>2</sub> active phases [29, 30]. CB surface area was increased

by oxidation in hot nitric acid for 24 h from 139 m<sup>2</sup>/g (bare CB) up to 323 m<sup>2</sup>/g (hereinafter CBox) and the micro-pores/meso-pores ratio modified increasing the volume of micro-pores. CBox was (i) tested as it is; (ii) thermally threated (annealing up to 800°C under inert atmosphere); (iii) grafted with amino groups, CBox-NH<sub>2</sub>; (iv) coated with iron oxide particles, CBox/FM (50 wt.%); and (v) impregnated with a triazole-based (trihexyl(tetradecyl)phosphonium triazole, [P66614][Triz]) ionic liquid (IL), CBox/IL. In the latter case, the sample obtained impregnating raw CB with IL (CB/IL) has been also produced for comparison [29, 30]. All the CB-based adsorbents were structurally and morphologically characterized [29]. The materials exhibit a good thermal stability (up to 600°C in the case of oxidized material, up to 200°C in the case of amino-functionalized material and IL-supported adsorbents, and up to 500°C in the case of iron oxide-containing composites) and a good variability in terms of surface areas and pore size distributions [29]. The CO<sub>2</sub> capture performances, evaluated in dynamic conditions in a lab-scale fixed bed micro-reactor operating at CO<sub>2</sub> 3 vol.% (inlet flow rate 15 Nl/h) and atmospheric pressure [29], allowed to estimate the material adsorption performances in dependence of the different textural properties of the carbonaceous support.

It was shown (**Figure 4**) that CBox and thermally annealed CBox exhibit lower sorption (8.8 and 11.1 mg<sub>CO2</sub>/g, respectively), the former comparable to CB [29, 30]. The sample obtained by CBox amine functionalization exhibits high CO<sub>2</sub> uptake despite its low surface area (29.5 m<sup>2</sup>/g) indicating a clear chemisorption adsorption mechanism [30].

The comparison among the samples obtained by covering CBox and CB with a CO<sub>2</sub> active phase (IL or FM) clearly indicates that the enhanced CBox micro-porosity greatly limits the accessibility of CO<sub>2</sub> toward the absorbing phase that is clogged into the micro-pores, lowering the number of available binding sites for CO<sub>2</sub> [29]. This effect is remarkable since the CO<sub>2</sub> uptake lowers from 18.3 mg<sub>CO2</sub>/g to 8.0 mg<sub>CO2</sub>/g in the case of FM-covered carbons (while the surface area increases from 156.7 in CB/FM to 247.6 m<sup>2</sup>/g in CBox/FM) and from 27.3 mg<sub>CO2</sub>/g to

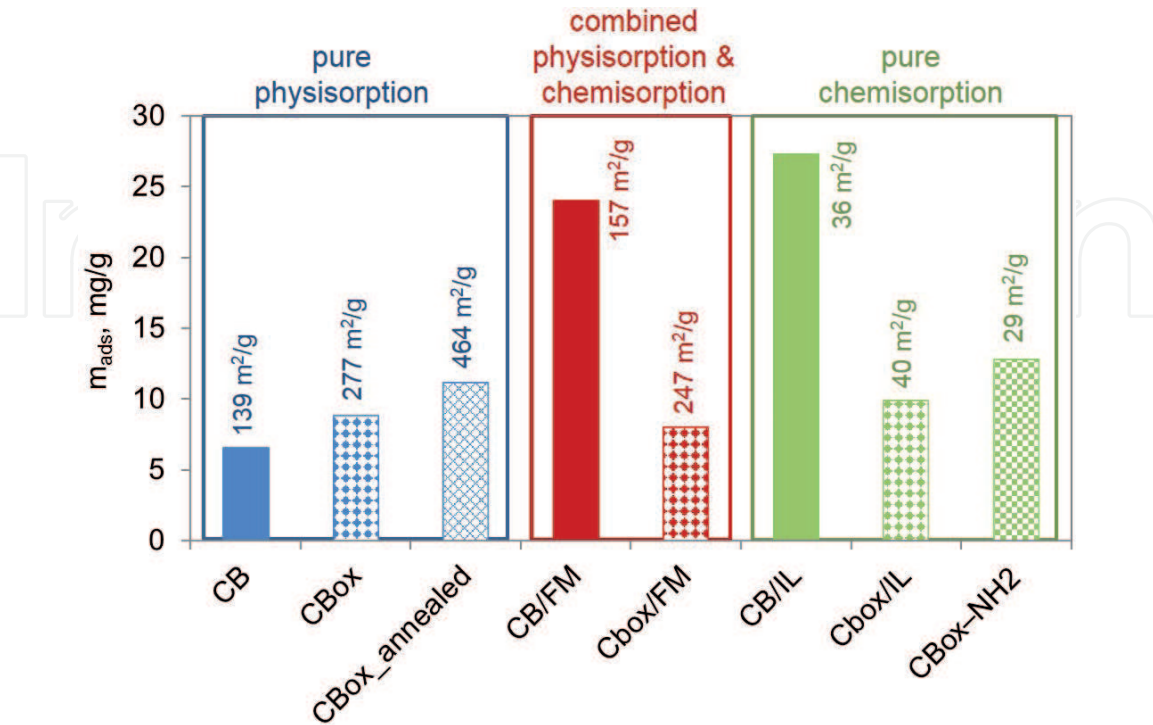


**Figure 4.** CO<sub>2</sub> sorption capacities ( $m_{ads}$ , mg/g) of the CB-derived hybrid materials. Experimental conditions: 0.35 g of adsorbent, lab-scale fixed bed micro-reactor, 3% CO<sub>2</sub> (inlet flow rate 15 Nl/h) in N<sub>2</sub>, room temperature, and pressure.

9.9 mg<sub>CO2</sub>/g in the case of IL-covered carbons (where the surface area keeps quite constant moving from 36.5 to 40.2 m<sup>2</sup>/g in CBox/FM and CBox/FM, respectively) (**Figure 4**) [29].

### 3. Highly CB destructure

#### 3.1 Graphene-like (GL) layers and ultrathin (GL) films

The destructure of the CB microstructure (achieved after 90 h of hot acidic treatment) allows obtaining two classes of water-stable materials placeable into the family of graphene-related materials (GRMs): (i) graphene-like (GL) layers [33, 34] and (ii) small graphenic fragments classifiable as carbon nanodots (CNDs) [35] exhibiting fluorescence in the visible region. The former class (hereinafter GL layers) can be easily obtained by chemical reduction of the product obtained after 90 h of acidic treatment [33, 34]. At the end of the oxidation step, the precursors of GL layers are recovered as a solid after centrifugation, while CNDs are recovered in the supernatant. The GL layer precursors are then converted into GL layers through a chemical reduction in mild conditions [33, 34]. The two-step (oxidation and reduction) approach is performed in aqueous medium and allows scalability and potentially large-amount production at reduced costs.

The morphological characterization of GL layers, performed by atomic force microscopy (AFM) on very diluted GL water suspension (0.1 µg/mL) [36], allowed to image rather individual GL layer units with vertical sizes ranging from about 1 nm or less to a few nanometers; the larger lateral dimensions, a few tens of nanometers, indicate that some aggregations are still occurring and that the primary aggregation process occurs to form preferentially extended thin planes [33].

Unlike rGO, whose basal planes are damaged at a different extent (formation of defects or holes) upon the removal of carbonyl and ether groups, the GL layers are characterized by intact graphenic basal planes. The edges of the GL graphenic layers are mainly decorated with a complex variety of oxygen functional groups (mainly carboxylic and carbonyl groups [33, 34]) giving to the GL layers an exceptional colloidal stability over a wide pH range (3–14) hardly achieved by conventional rGO without using stabilizing agents.

The quantification of the oxygen functional groups by coulometric-potentiometric titration in the pH range of 2.7–7 [34] allows identifying two dominant classes in the carboxylate region (pK 2.0–5.0) with pK<sub>a</sub> = 3.40 ± 0.05 (number of sites = 900 ± 30 µmol/g) and pK<sub>a</sub> = 5.5 ± 0.1 (number of sites = 240 ± 30 µmol/g, mainly lactones and carboxylic anhydride groups) [34].

An intriguing aspect of GL is related to its wide chemical versatility that allowed the production of different kinds of hybrid materials. Different materials have been produced and explored for a wide array of applications: metal organic frameworks (MOF)/GL hybrids have been obtained allowing MOF to grow in presence of GL layers [37], biocompatible hybrids have been developed interfacing eumelanin and GL layers (EUGLs) [38, 39], and photocatalytic hybrids have been produced by interfacing TiO<sub>2</sub> and GL layers [40, 41].

Interestingly enough, the GL layers exhibit a peculiar self-assembling behavior when dried on surfaces, arranging in different morphologies (ranging from atomically flat to patterned surface) as a consequence of the suspension pH, surface roughness, and chemistry [34]. Thanks to their peculiar characteristics, GL layers are also particularly suitable to homogeneously coat non-planar surfaces, including particles (TiO<sub>2</sub>, silica, Al<sub>2</sub>O<sub>3</sub>) and living cells [36]. When GL layers are contacted with planktonic *S. aureus* living cells [36], they exhibit antimicrobial activity and



are also capable to inhibit the formation of *S. aureus* biofilm. It was found that the antimicrobial capabilities were exerted without altering the integrity of the plasma membrane, reasonably by simply coating the cell membrane likely mediated by electrochemical interactions between the GL-derived functional groups and cell wall/plasma membrane proteins. The scavenging activity of GL layers has also been found [40], while bare rGO was beyond the detection limit. Electron paramagnetic resonance (EPR) spectroscopy investigation on GL layers showed a single and asymmetric signal at g-values of  $\sim 2.0035$  (spin density =  $4.3 \times 10^{18}$  spin/g, signal amplitude  $\Delta B = 3.4 \pm 0.2$ ) typical of carbon-centered radicals and related to the localized spins generated at the edge of the  $\pi$ -electron system [40, 41].

The presence of quite intact basal plane in GL layers guarantees electrical conductivity. I-V characterization showed linear responses implying an Ohmic behavior of GL films. The conductivity of a GL film of around 20 nm height, estimated by the classical four-probe van der Pauw configuration [42], was  $2.5 \pm 0.3 \times 10^{-2}$  S/cm [33]. This characteristic was successfully exploited to prepare conductive hybrid materials in water suspension [37–41].

### 3.2 VOC sensing

The good conductivity exhibited by GL layers combined with the tendency to form differently patterned films was exploited also for the development of prototypal devices for sensoristic applications in volatile organic compound (VOC) detection, paying a particular attention to alcohol detection [43, 44].

The need of low-cost, eco-compatible VOC sensors for the air quality monitoring working at room temperature [45] pushes research activities toward the constant development and testing of new sensing layers. In the manifold of nano-materials suitable for developing a gas sensor, GRMs attract increasing interest, since they combine excellent detection sensitivity with transduction properties and easily tunable chemo-physical characteristics [45, 46].

The performances of GL films as sensing layers were probed at first using a prototypal chemoresistive device prepared by drop-casting GL solution onto alumina-based transducers and dried at room temperature. The ability to detect alcohol vapors (ethanol and n-butanol) was evaluated at atmospheric pressure, room temperature, and dried atmosphere, in the range of 0–100 ppm. After conditioning for 30 min in dry air (baseline), the sensing device was exposed to analytes for a time ranging between 10 and 30 min and then restored for a time ranging between 20 and 60 min (**Figure 5**).

The GL layer response toward ethanol depends on the reduction strategy adopted (hydrazine hydrate or NMP refluxing [43]) and, expressed as normalized relative variation of conductance, it varies from 3% to 6% for ethanol at 50 ppm and from 0.5% to 1.1% for n-butanol (**Figure 5**) at 50 ppm, where the lower values are referred to GL layers reduced with hydrazine hydrate and the higher responses are referred to GL layers reduced with NMP refluxing [43]. The response of the GL precursors was also reported for comparison (**Figure 5**).

Overall, the lower response to n-butanol than that to ethanol could be ascribed to the different ability of both alcohols to permeate the GL flakes (the analytes have a different steric hindrance), as well as to the different chemical affinity to functional groups on the GL layer surfaces. A combined role of morphology and surface chemistry in determining the response to the analytes was assumed as a possible interpretation of experimental evidences [43].

The device was also tested at increasing concentration steps of ethanol and butanol [43] up to a concentration of 100 ppm (lower panels of **Figure 5**). The tests clearly showed that the sensing response increased according to the increasing



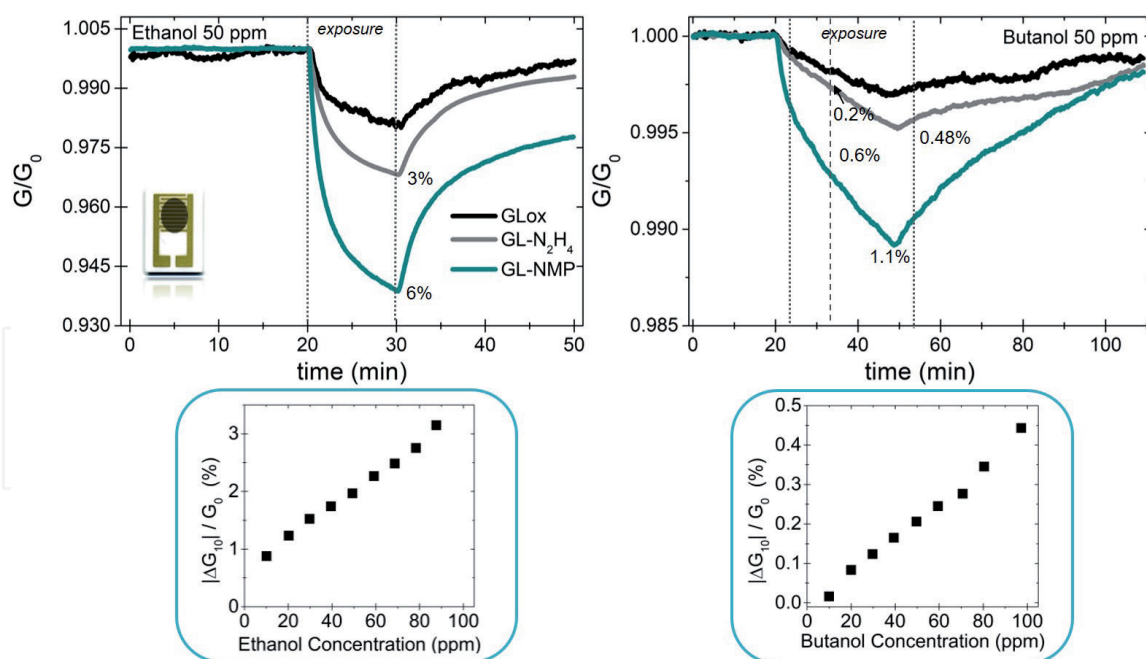


**Figure 5.**

Responses of the chemoresistive devices based on GLox (black curve), GL- $\text{N}_2\text{H}_4$  film (gray curve), and GL-NMP film (blue curve) toward ethanol (upper panel) and n-butanol (lower panel) vapors. The device responses at increasing concentration (up to 100 ppm) of ethanol and butanol are reported in the lower panels. Adapted from [43].

analyte concentration [43] and that the prototypal devices are able to discriminate between different concentrations. The higher sensitivity toward ethanol is confirmed at all the concentrations explored reaching, in the case of GL layers reduced with NMP refluxing, around 1% at 10 ppm of ethanol.

The comparison of the experimental results with those reported by literature showed that GL films are a promising candidate for the detection of low concentrations of ethanol at room temperature [43].

Starting on these encouraging results, preliminary attempts to process GL layers from aqueous suspension in finely controlled paths by means of inkjet printing (IJP) manufacturing have been performed [44]. The IJP technology is a deposition method from liquid phase that well addresses the demand for fine patterning necessary for sensoristic applications [47]. The IJP technology permits an efficient use of nonflexible and flexible eco-friendly substrates (as paper substrates) reducing the amount of waste products [47] by ensuring i) effective control on the deposited ink volume; ii) no-vacuum, no-temperature, and contactless deposition; iii) high reproducibility [47].

Prototypal chemoresistors have been fabricated by printing GL layers onto glossy paper with interdigitated Cr/Au electrodes as a rectangular surface [44]. The printing parameters have been optimized in order to obtain uniform, conductive, and reproducible sensing films (**Figure 6**). In order to assess the reproducibility of the deposition technique, two twin devices were fabricated, and in both devices the sensing GL-based film has been realized by printing multiple overlapped layers.

The sensing properties of the printed GL layer prototypal chemoresistors have been investigated by exposing them to vapors of ethanol under the same conditions reported above (**Figure 6**). The response toward ethanol (50 ppm, in dry  $\text{N}_2$ ) in terms of conductance variation was 1.3%. Intra-substrate reproducibility in terms of surface morphology (macroscopic and microscopic distribution of the printed nanomaterial) and electrical responses (base resistance and conductance variation) was also demonstrated [44].

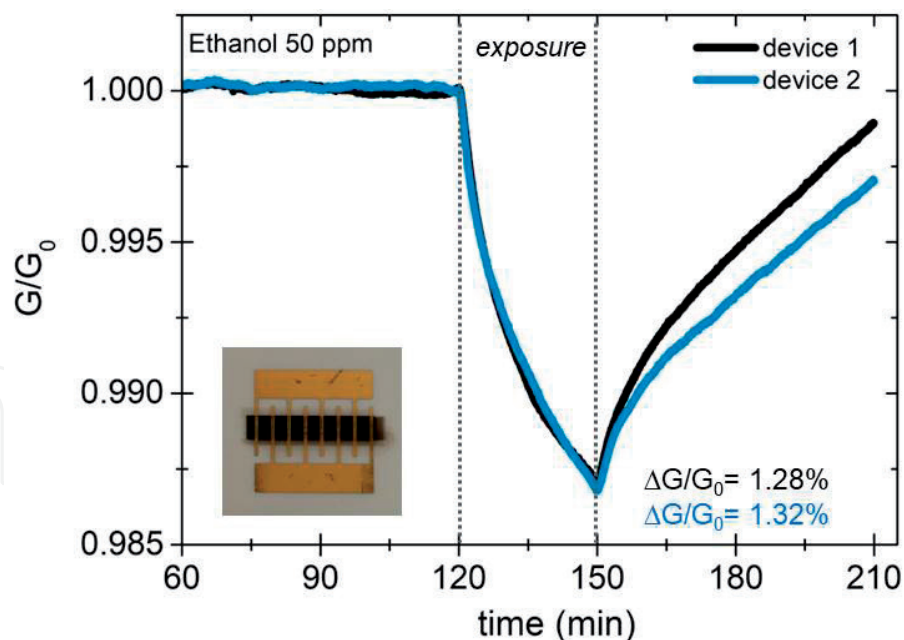


**Figure 6.**  
*Responses of the twin GL-N<sub>2</sub>H<sub>4</sub>-based chemoresistive devices produced by IJP toward ethanol vapors. Adapted from [44].*

The possibility to use different substrates (alumina, silicon dioxide) is currently under study with the aim of evaluating the more suitable substrate for GL-based chemoresistor production.

## 4. Conclusions

This chapter reports the very recent experimentation aimed to valorize the potentialities of carbon black for practical and uncommon applications. The proposed approaches are purposively designed to be simple, cost-effective, versatile, suitable for synthesis scale-up, and, possibly, sustainable (quite mild synthesis conditions, where water is mostly used as solvent). The approaches have been developed taking into account the relationships between CB-derived carbons nanostructuration (i.e., micro-/meso-pore ratio, specific surface chemistry, etc.) and macroscopic properties.

It was shown that CB can be modified on the surface (preserving the micro-structure) and fully destructured until separating the graphenic building blocks embedded in. The preserved conductive properties allow the exploitation of the graphenic layers (graphene-like layers) for VOC sensing application, thus avoiding the use of metal oxides for this specific application in view of more sustainable sensors. Applications in CO<sub>2</sub> capture and storage (CCS) and water remediation (heavy metal capture and rare-earth element recovery) of CB modified at the surface resulted encouraging and mature for practical applications.

## Acknowledgements

This paper is based on the collaboration with Roberto Di Capua, Fulvia Villani, Tiziana Polichetti, Francesco di Natale, Paola Ammendola, Federica Raganati, and Luciana Lisi since many years.

## **Conflict of interest**

The authors declare no conflict of interest.

IntechOpen


IntechOpen

## **Author details**

Michela Alfè\* and Valentina Gargiulo  
Institute for Research on Combustion (IRC-CNR), Naples, Italy

\*Address all correspondence to: [alfe@irc.cnr.it](mailto:alfe@irc.cnr.it)

## **IntechOpen**

© 2020 The Author(s). Licensee IntechOpen. Distributed under the terms of the Creative Commons Attribution - NonCommercial 4.0 License (<https://creativecommons.org/licenses/by-nc/4.0/>), which permits use, distribution and reproduction for non-commercial purposes, provided the original is properly cited. 

## References

- [1] Long CM, Nascarella MA, Valberg PA. Carbon black vs. black carbon and other airborne materials containing elemental carbon: Physical and chemical distinctions. *Environmental Pollution*. 2013;**181**:271-286. DOI: 10.1016/j.envpol.2013.06.009
- [2] Fan Y, Fowler GD, Zhao M. The past, present and future of carbon black as a rubber reinforcing filler: A review. *Journal of Cleaner Production*. 2020;**247**:119115. DOI: 10.1016/j.jclepro.2019.119115
- [3] Watson AY, Valberg PA. Carbon black and soot: Two different substances. *AIHA Journal*. 2001;**62**(2):218-228. DOI: 10.1080/15298660108984625
- [4] Arnal C, Alfè M, Gargiulo V, Ciajolo A, Alzueta MU, Millera A, et al. Characterization of soot. In: Battin-Leclerc F, Simmie JM, Blurock E, editors. *Cleaner Combustion-Developing Detailed Chemical Kinetic Models*. Springer Nature Switzerland; 2013. pp. 333-362
- [5] Boehm HP. Some aspects of the surface chemistry of carbon blacks and other carbons. *Carbon*. 1994;**32**(5):759-769. DOI: 10.1016/0008-6223(94)90031-0
- [6] Mannfredi C, Mozzillo R, Volino S, Trifuoggi M, Giarra A, Gargiulo V, et al. On the modeling of heavy metals and rare earth elements adsorption on colloidal carbon-based nanoparticles. *Applied Surface Science*. 2020;**505**:144264. DOI: 10.1016/j.apsusc.2019.144264
- [7] Lounasvuori MM, Kelly D, Foord JS. Carbon black as low-cost alternative for electrochemical sensing of phenolic compounds. *Carbon*. 2018;**129**:252-257. DOI: 10.1016/j.carbon.2017.12.020
- [8] Wu C-S, Chang T-W, Teng H, Lee Y-L. High performance carbon black counter electrodes for dye-sensitized solar cells. *Energy*. 2016;**115**:513-518. DOI: 10.1016/j.energy.2016.09.052
- [9] Liu D, Zhao X, Song L, Zhang S. Synthesis, performance and action mechanism of carbon black/Ag<sub>3</sub>PO<sub>4</sub> photocatalysts. *Ceramics International*. 2018;**44**:13712-13719. DOI: 10.1016/j.ceramint.2018.04.212
- [10] Kokhanovskaya OA, Razdyakonova GI, Likholobov VA. New applications of carbon black. An aerogel-like composite material with heat insulating properties. *Procedia Engineer*. 2016;**152**:540-544. DOI: 10.1016/j.proeng.2016.07.652
- [11] Pahalagedara LR, Siriwardane IW, Tissera ND, Wijesena RN, Nalin de Silva KM. Carbon black functionalized stretchable conductive fabrics for wearable heating applications. *RSC Advances*. 2017;**7**:19174-19180. DOI: 10.1039/C7RA02184D
- [12] Chen B, Li B, Gao Y, Ling T-C, Lu Z, Li Z. Investigation on electrically conductive aggregates produced by incorporating carbon fiber and carbon black. *Construction and Building Materials*. 2017;**144**:106-114. DOI: 10.1016/j.conbuildmat.2017.03.168
- [13] Monteiro AO, Loreda A, Costa PMFJ, Oeser M, Cachim PB. A pressure-sensitive carbon black cement composite for traffic monitoring. *Construction and Building Materials*. 2017;**154**:1079-1086. DOI: 10.1016/j.conbuildmat.2017.08.053
- [14] Santini E, Ravera F, Ferrari M, Alfè M, Ciajolo A, Liggieri L. Interfacial properties of carbon particulate-laden liquid interfaces and stability of related foams and emulsions. *Colloid Surface A*. 2010;**365**(1-3):189-198. DOI: 10.1016/j.colsurfa.2010.01.041



- [15] Gargiulo V, Alfè M, Lisi L, Manfredi C, Volino S, Di Natale F. Colloidal carbon-based nanoparticles as heavy metal adsorbent in aqueous solution: Cadmium removal as a case study. *Water, Air, & Soil Pollution*. 2017;**228**(5):192-205. DOI: 10.1007/s11270-017-3378-5
- [16] Alfe M, Gargiulo V, Di Capua R. An old but lively nanomaterial: Exploiting carbon black for the synthesis of advanced materials. *Eurasian Chemico-Technological Journal*. 2019;**21**(3):203-213. DOI: 10.18321/ectj861
- [17] Di Natale F, Gargiulo V, Alfè M. Adsorption of heavy metals on silica-supported hydrophilic carbonaceous nanoparticles (SHNPs). Accepted on *Journal of Hazardous Materials*. 2020. DOI: 10.1016/j.jhazmat.2020.122374
- [18] Decreto Legislativo 3 aprile 2006, n. 152. Available from: <http://www.camera.it/parlam/leggi/deleghe/06152dl.htm>
- [19] Alfarra A, Frackowiak E, Béguin F. The HSAB concept as a means to interpret the adsorption of metal ions onto activated carbons. *Applied Surface Science*. 2004;**228**:84-92. DOI: 10.1016/j.apsusc.2003.12.033
- [20] Leung DY, Caramanna G, Maroto-Valer MM. An overview of current status of carbon dioxide capture and storage technologies. *Renewable and Sustainable Energy Reviews*. 2014;**39**:426-443. DOI: 10.1016/j.rser.2014.07.093
- [21] Samanta A, Zhao A, Shimizu GKH, Sarkar P, Gupta R. Post-combustion CO<sub>2</sub> capture using solid sorbents: A review. *Industrial and Engineering Chemistry Research*. 2012;**51**:1438-1463. DOI: 10.1021/ie200686q
- [22] D'Alessandro DM, Smit B, Long JR. Carbon dioxide capture: Prospects for new materials. *Angewandte Chemie International Edition*. 2012;**49**:6058-6082. DOI: 10.1002/anie.201000431
- [23] Nugent P, Belmabkhout Y, Burd SD, Cairns AJ, Luebke R, Forrest RK, et al. Porous materials with optimal adsorption thermodynamics and kinetics for CO<sub>2</sub> separation. *Nature*. 2013;**495**:80-84. DOI: 10.1038/nature11893
- [24] Oschatz M, Antonietti M. A search for selectivity to enable CO<sub>2</sub> capture with porous adsorbents. *Energy & Environmental Science*. 2018;**11**:57-70. DOI: 10.1039/C7EE02110K
- [25] Baltrusaitis J, Jensen JH, Grassian VH. FTIR spectroscopy combined with isotope labeling and quantum chemical calculations to investigate adsorbed bicarbonate formation following reaction of carbon dioxide with surface hydroxyl groups on Fe<sub>2</sub>O<sub>3</sub> and Al<sub>2</sub>O<sub>3</sub>. *The Journal of Physical Chemistry. B*. 2006;**110**:12005-12016. DOI: 10.1021/jp057437j
- [26] Mishra AK, Ramaprabhu S. Nano magnetite decorated multiwalled carbon nanotubes: A robust nanomaterial for enhanced carbon dioxide adsorption. *Energy & Environmental Science*. 2011;**4**:889-895. DOI: 10.1039/C0EE00076K
- [27] Mishra AK, Ramaprabhu S. Magnetite decorated graphite nanoplatelets as cost effective CO<sub>2</sub> adsorbent. *Journal of Materials Chemistry*. 2011;**21**:7467-7471. DOI: 10.1039/C1JM10996K
- [28] Alfè M, Ammendola P, Gargiulo V, Raganati F, Chirone R. Magnetite loaded carbon fine particles as low-cost CO<sub>2</sub> adsorbent in a sound assisted fluidized bed. *Proceedings of the Combustion Institute*. 2015;**35**:2801-2809. DOI: 10.1016/j.proci.2014.06.037
- [29] Gargiulo V, Alfè M, Ammendola P, Raganati F, Chirone R. CO<sub>2</sub> sorption

on surface-modified carbonaceous support: Probing the influence of the carbon black microporosity and surface polarity. *Applied Surface Science*. 2016;**360**:329-337. DOI: 10.1016/j.apsusc.2015.11.026

[30] Gargiulo V, Alfè M, Raganati F, Zhumagaliyeva A, Doszhanov Y, Ammendola P, et al. CO<sub>2</sub> adsorption under dynamic conditions: An overview on rice husk-derived sorbents and other materials. *Combustion Science and Technology*. 2018;**191**(9):1484-1498. DOI: 10.1080/00102202.2018.1546697

[31] Raganati F, Alfe M, Gargiulo V, Chirone R, Ammendola P. Isotherms and thermodynamics of CO<sub>2</sub> adsorption on a novel carbon-magnetite composite sorbent. *Chemical Engineering Research and Design*. 2018;**134**:540-552. DOI: 10.1016/j.cherd.2018.04.037

[32] Raganati F, Alfe M, Gargiulo V, Chirone R, Ammendola P. Kinetic study and breakthrough analysis of the hybrid physical/chemical CO<sub>2</sub> adsorption/desorption behavior of a magnetite-based sorbent. *Chemical Engineering Journal*. 2019;**372**:526-535. DOI: 10.1016/j.cej.2019.04.165

[33] Alfè M, Gargiulo V, Di Capua R, Chiarella F, Rouzaud J-N, Vergara A, et al. Wet chemical method for making graphene-like films from carbon black. *ACS Applied Materials & Interfaces*. 2012;**4**:4491-4498. DOI: 10.1021/am301197q

[34] Alfè M, Gargiulo V, Di Capua R. Tuning the surface morphology of self-assembled graphene-like thin films through pH variation. *Applied Surface Science*. 2015;**353**:628-635. DOI: 10.1016/j.apsusc.2015.06.117

[35] Dong Y, Chen C, Zheng X, Gao L, Cui Z, Yang H, et al. One-step and high yield simultaneous preparation of single- and multi-layer graphene

quantum dots from CX-72 carbon black. *Journal of Materials Chemistry*. 2012;**22**:8764-8766. DOI: 10.1039/c2jm30658a

[36] Olivi M, Alfè M, Gargiulo V, Valle F, Mura F, Di Giosia M, et al. Antimicrobial properties of graphene-like nanoparticles: Coating effect on *Staphylococcus aureus*. *Journal of Nanoparticle Research*. 2016;**18**(12):358. DOI: 10.1007/s11051-016-3673-x

[37] Alfè M, Gargiulo V, Lisi L, Di Capua R. Synthesis and characterization of conductive copper-based metal-organic framework/graphene-like composites. *Materials Chemistry and Physics*. 2014;**147**:744-750. DOI: 10.1016/j.matchemphys.2014.06.015

[38] Gargiulo V, Alfè M, Di Capua R, Togna AR, Cammisotto V, Fiorito S, et al. Supplementing  $\pi$ -systems: Eumelanin and graphene-like integration towards highly conductive materials for the mammalian cell culture bio-interface. *Journal of Materials Chemistry B*. 2015;**3**:5070-5079. DOI: 10.1039/C5TB00343A

[39] Di Capua R, Gargiulo V, Alfè M, De Luca GM, Skála T, Mali G, et al. Eumelanin graphene-like integration: The impact on physical properties and electrical conductivity. *Frontiers in Chemistry*. 2019;**7**:121. DOI: 10.3389/fchem.2019.00121

[40] Lettieri S, Gargiulo V, Pallotti DK, Vitiello G, Maddalena P, Alfè M, et al. Evidencing opposite charge-transfer processes at TiO<sub>2</sub>/graphene-related materials interface through a combined EPR, photoluminescence and photocatalysis assessment. *Catalysis Today*. 2018;**315**:19-30. DOI: 10.1016/j.cattod.2018.01.022

[41] Alfè M, Spasiano D, Gargiulo V, Vitiello G, Di Capua R, Marotta R. TiO<sub>2</sub>/graphene-like photocatalysts for selective oxidation of 3-pyridine-methanol to

vitamin B3 under UV/solar simulated radiation in aqueous solution at room conditions: The effect of morphology on catalyst performances. *Applied Catalysis A: General*. 2014;**487**:91-99. DOI: 10.1016/j.apcata.2014.09.002

[42] Van Der Pauw LJ. A method of measuring specific resistivity and Hall effect of discs of arbitrary shape. *Philips Research Reports*. 1958;**13**:1-9

[43] Gargiulo V, Alfano B, Di Capua R, Alfé M, Vorokhta M, Polichetti T, et al. Graphene-like layers as promising chemoresistive sensing material for detection of alcohols at low concentration. *Journal of Applied Physics*. 2018;**123**(2):024503. DOI: 10.1063/1.5000914

[44] Villani F, Loffredo F, Alfano B, Miglietta ML, Verdoliva L, Alfè M, et al. Graphene-like based-chemoresistors inkjet-printed onto paper substrate. In: Leone A, Forleo A, Francioso L, Capone S, Siciliano P, Di Natale C, editors. *Sensors and Microsystems: Proceedings of the 19th AISEM 2017 National Conference (Lecture Notes in Electrical Engineering)*. Springer Nature Switzerland; 2019

[45] Baptista FR, Belhout SA, Giordani S, Quinn SJ. Recent developments in carbon nanomaterial sensors. *Chemical Society Reviews*. 2015;**44**:4433-4453. DOI: 10.1039/C4CS00379A

[46] Llobet E. Gas sensors using carbon nanomaterials: A review. *Sensors and Actuators, B: Chemical*. 2013;**179**:32

[47] Singh M, Haverinen HM, Dhagat P, Jabbour GE. Inkjet printing—Process and its applications. *Advanced Materials*. 2010;**22**:673-685. DOI: 10.1002/adma.200901141